Design and analysis of photonic crystal structures for dual-band transmission in optical communication

SHICONG HU, MINGWEI MEI, HUAJUN YANG*, PING JIANG, WEINAN CAIYANG, LIQIONG QIAN
College of Physical Electronics, University of Electronic Science and Technology of China, Sichuan Province, China

The modified binary one-dimensional photonic crystal (MB-1DPC), ternary 1DPC (T-1DPC) and heterostructured ternary 1DPC (HT-1DPC) are investigated to achieve the omnidirectional total reflection in the free-space optical communication dual-band range of 810 nm ~ 910 nm and 1550 nm ~ 1610 nm. With material absorption, the reflectivity in the dual-band range for the binary 1DPC (B-1DPC), MB-1DPC, T-1DPC, and HT-1DPC have been studied. The maximum value of reflectivity in each structure that can be achieved in the dual-band range is determined by the TM polarization. The highest reflectivity can reach up to 99.62% for TM mode by employing HT-1DPC multilayers, which is composed of Si, As_2Se_3 and SiO_2.

(Received August 7, 2017; accepted April 5, 2018)

Keywords: Photonic crystals, Omnidirectional total reflection, Free-space optical communication

1. Introduction

PCs were firstly introduced in 1978 [1]. Over the past two decades, there has been an increasing interest in the investigation of PCs that are characterized by photonic crystal band-gaps (PBGs). It has been demonstrated in previous articles that the omnidirectional total reflection wavelength range can been enhanced by using photonic heterostructures [2, 3]. The aperiodic or quasi-periodic PC is an effective and simple approach for broadening the PBGs in periodically stratified medium. On the other hand, PCs with PBGs have been intensively investigated with different materials such as negative index material [4, 5], plasma [6, 7], metal [8], anisotropic material [9-11], graded index material [12-16], etc.

Metallic reflector can reflect light for arbitrary incident angles over a wide range of frequencies. However, a metallic reflector has a vast power loss due to the absorption at infrared or higher frequencies. Due to the characteristic of low loss, omnidirectional reflectors of PCs have potential application in microcavity [17], Bragg fibers [18-21], Fabry–Perot resonators [22], etc. In the case of material absorption, the omnidirectional photonic crystal band-gap (OPBG) no longer exists in the strict sense. Early paper [23] on multilayer reflector discussed the properties for the reflectance, which is independent of the number N of the stratifications and the properties of the substrate, provided N is large enough.

Antenna systems coated with multilayer film have been investigated to improve the transmission efficiency of long-range communication [24-26]. Much attention has been given to the investigation of an OPBG and its bandwidth enhancement in the absence of material absorption [2-3, 7, 27-28]. Papers [24, 29] on antenna systems only considered the 1550 nm band in optical communication. In this paper, design and analysis of several PC multilayered structures are investigated to achieve high reflectivity in the dual-band range, i.e., 810 nm ~ 910 nm and 1550 nm ~ 1610 nm, which involve the wavelengths of the beacon light and the signal light in optical communication, respectively. The omnidirectional total reflection in the dual-band range for TE mode and TM mode should be studied. Since the OPBG of TM mode is narrower than the TE one apart from the normal incidence, the bandwidth of the omnidirectional reflector is determined by the OPBGs of TM mode. Our study is carried out in two aspects. Firstly, MB-1DPC, T-1DPC and HT-1DPC have been investigated to achieve the omnidirectional total reflection from 810 nm to 910 nm and from 1550 nm to 1610 nm without material absorption for TM mode. In addition, the effects of the refractive indices and the structural parameters of the PCs on the wavelength range and bandwidths of the two OPBGs have been discussed. The simulation results indicate the bandwidth of the two OPBGs can be considerably enhanced by using the HT-1DPC. On the other hand, the reflectivity of the three structures and the B-1DPC in the two optical communication bands of 810 nm ~ 910 nm and 1550 nm ~ 1610 nm has been discussed in the regime of the material absorption. Therefore, the PCs multilayer film can be applied in Cassegrain antenna with reflectivity type primary mirror and secondary mirror.

2. Theoretical model and method

In this section, the model and theoretical method of the MB-1DPC, T-1DPC and HT-1DPC are introduced.

2.1. Theoretical Model

The MB-1DPC is composed of alternate layers of high refractive index n_H and low refractive index n_L, as shown in Fig. 1(a) [30]. Each period of HT-1DPC is composed of three layers, the refractive indices of which are presented by n_H, n_M and n_L, respectively. The index profile of

T-1DPC and HT-1DPC are shown in Fig. 1(b). In Fig. 1, x axis represents the normal direction of the primary mirror and secondary mirror of Cassegrain antenna.

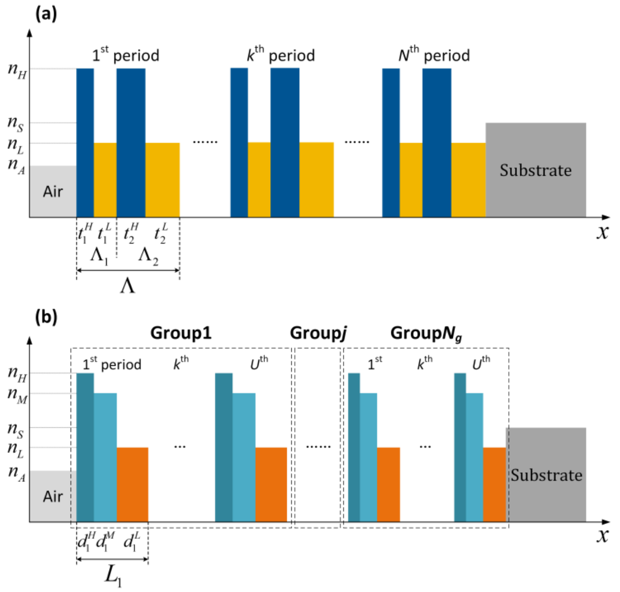

Fig. 1. (a) Index profile of MB-1DPC. (b) Index profile of HT-1DPC.

In Fig. 1(a), The thicknesses of the high (low) refractive index layers in one period for MB-1DPC structure are denoted by t_1^H (t_1^L) and t_2^H (t_2^L), respectively. The period in MB-1DPC is denoted by $\Lambda = \Lambda_1 + \Lambda_2$ and consists of two bilayers, the thicknesses of which are denoted by $\Lambda_1 = t_1^H + t_1^L$ and $\Lambda_2 = t_2^H + t_2^L$, respectively. The number of periods contained is denoted by N. Fig. 1(b) represents the index profile of HT-1DPC with group $N_g > 1$. HT-1DPC consists of different groups and the number of unit cells contained in the jth group is donated by N_j, the period of which is denoted by $L_j = d_j^H + d_j^M + d_j^L$. Each group has the same structure (T-1DPC). The thickness of the period is denoted by $L_1 = d_1^H + d_1^M + d_1^L$. In HT-1DPC and T-1DPC, the number of periods contained is denoted by U, The indices of air and substrate in these two structures are denoted by n_A and n_S, respectively.

2.2. Theoretical method

2.2.1. Theoretical Method of Photonic Crystal Band-gap

The Transfer Matrix Method (TMM) [31] is used to analyze the PBG characteristics of both MB-1DPC and T-1DPC consisting of only one group, i.e., T-1DPC with $N_g = 1$. The method which employs TMM and Bloch-Floquet theorem drives eigenvalue equations, which is given by

$$\exp(iK_{TM}T) = \mathrm{Re}(A_{TM}) \pm \sqrt{[\mathrm{Re}(A_{TM})]^2 - 1} \tag{1}$$

$$\exp(iK_{TE}T) = \mathrm{Re}(A_{TE}) \pm \sqrt{[\mathrm{Re}(A_{TE})]^2 - 1} \tag{2}$$

where K_{TE} and K_{TM} represents Bloch wavenumber of TE mode and TM mode, respectively. A_{TM} or A_{TE} has different forms in MB-1DPC and T-1DPC. T represents the period Λ of MB-1DPC or the period L_1 of T-1DPC. Since a real K_{TE} or K_{TM} determines an allowed mode and an imaginary K_i determines a forbidden mode, the allowed modes can be determined by the condition

$$|\mathrm{Re}(A_{TM})| < 1, |\mathrm{Re}(A_{TE})| < 1 \tag{3}$$

according to Eq. (3), Eqs. (1) and (2) can be simplified as

$$\cos(K_{TM}T) = \mathrm{Re}(A_{TM}) \tag{4}$$

$$\cos(K_{TE}T) = \mathrm{Re}(A_{TE}) \tag{5}$$

2.2.2. Theoretical Method of Reflectivity Spectra

The characteristic matrix [28] of the kth period is given by

$$M_k^j = \prod_{i=1}^{l} \begin{bmatrix} \cos\alpha_i^j & \dfrac{-i\sin\alpha_i^j}{\eta_i} \\ -i\eta_i \sin\alpha_i^j & \cos\alpha_i^j \end{bmatrix} = \begin{bmatrix} M_{11}^j & M_{12}^j \\ M_{21}^j & M_{22}^j \end{bmatrix} \tag{6}$$

where l=4 (i=1,2,3,4 signify the layers of thicknesses t_1^H, t_1^L, t_2^H and t_2^L, respectively) for MB-1DPC and l=3 (i=1,2,3 signify the layers of thicknesses d_1^H, d_1^M and d_1^L, respectively) for T-1DPC when $j = 1$, and l=3 (i=1,2,3 signify the layers of thicknesses d_j^H, d_j^M and d_j^L, respectively) for HT-1DPC when $j > 1$.

$$\eta_i = \begin{cases} n_i \cos(\theta_i) & \text{for TE mode} \\ \cos(\theta_i)/n_i & \text{for TM mode} \end{cases} \tag{7}$$

$$\alpha_i = (2\pi/\lambda_0) n_i t_i \cos(\theta_i) \quad \text{for MB-1DPC} \tag{8}$$

$$\alpha_i^j = (2\pi/\lambda_0) n_i d_i^j \cos(\theta_i) \quad \text{for HT-1DPC} \tag{9}$$

where θ_i stands for the ray angle inside the layers of thicknesses t_i or d_j^i. The characteristic matrix of the entire photonic crystal is given by

$$M = \prod_{j=1}^{N_g}\prod_{k=1}^{N_j} M_k^j = \prod_{j=1}^{N_g} \begin{bmatrix} M_{11}^j \sigma_{N_j-1}(a_j) - \sigma_{N_j-2}(a_j) & M_{12}^j \sigma_{N_j-1}(a_j) \\ M_{21}^j \sigma_{N_j-1}(a_j) & M_{22}^j \sigma_{N_j-1}(a_j) - \sigma_{N_j-2}(a_j) \end{bmatrix} = \begin{bmatrix} m_{11} & m_{12} \\ m_{21} & m_{22} \end{bmatrix} \tag{10}$$

where $\sigma_N(a_j)$ is the Chebyshev polynomials of the second kind, which is given by

$$\sigma_N(a_j) = \frac{\sin[(N+1)\cos^{-1}(a_j)]}{(1-a_j{}^2)^{1/2}} \tag{11}$$

where

$$a_j = \frac{1}{2}(M_{11}^j + M_{22}^j) \tag{12}$$

The reflection coefficient of the multilayer is given by

$$r = \frac{(m_{11}+\eta_{out}m_{12})\eta_{in} - (m_{21}+\eta_{out}m_{22})}{(m_{11}+\eta_{out}m_{12})\eta_{in} + (m_{21}+\eta_{out}m_{22})} \tag{13}$$

where

$$\eta_{in} = n_A\cos\theta_{in}, \eta_{out} = n_S\cos\theta_{out} = n_S\sqrt{1-\frac{n_A^2\sin^2\theta_{in}}{n_S^2}} \tag{14}$$

where θ_{in} and θ_{out} represent the incident angle in the air and the refraction angle in the substrate, respectively. The reflectivity of the multilayer media is given by

$$R = rr^* = |r|^2 \tag{15}$$

3. Analysis of the OPBGs without material absorption

The wavelength range of OPBG is determined by the contrast of refractive indices between composite structures of PCs [32, 33]. Namely, the bandwidth increases with the refractive contrast increases. Thus, the refractive contrast should be large enough to achieve the omnidirectional total reflection in two optical communication ranges from 810 nm to 910 nm and from 1550 nm to 1610 nm without material absorption. The refractive indices of the materials $n_H = 4.7$ (PbTe) [34], $n_M = 4.45$ (PbS) [35], $n_S = 2.9$ (As_2Se_3) [36] and $n_L = 1.46$ (BaF_2) [28] are selected in T-1DPC and MB-1DPC, as shown in Fig. 1.

3.1. Wavelength Range and Bandwidth of OPBGs in MB-1DPC

In Eqs. (1) and (2), the $\mathrm{Re}(A_{TM})$ for TM mode and the $\mathrm{Re}(A_{TE})$ for TE mode in MB-1DPC are given by

$$\begin{aligned}\mathrm{Re}(A_{TE}) = {} & \cos[k_H(t_1^H+t_2^H)]\cdot[\cos(k_Lt_2^L)\cos(k_Lt_1^L) \\ & -\frac{1}{4}(\frac{k_H}{k_L}+\frac{k_L}{k_H})^2\sin(k_Lt_2^L)\sin(k_Lt_1^L)] \\ & -\frac{1}{2}\sin[k_H(t_1^H+t_2^H)]\sin[k_L(t_1^L+t_2^L)](\frac{k_H}{k_L}+\frac{k_L}{k_H}) \\ & +\frac{1}{4}\cos[k_H(t_2^H-t_1^H)](\frac{k_H}{k_L}-\frac{k_L}{k_H})^2\sin(k_Lt_2^L)\sin(k_Lt_1^L)\end{aligned} \tag{16}$$

$$\begin{aligned}\mathrm{Re}(A_{TM}) = {} & \cos[k_H(t_1^H+t_2^H)]\cdot[\cos(k_Lt_2^L)\cos(k_Lt_1^L) \\ & -\frac{1}{4}(\frac{n_L^2k_H}{n_H^2k_L}+\frac{n_H^2k_L}{n_L^2k_H})^2\sin(k_Lt_2^L)\sin(k_Lt_1^L)] \\ & -\frac{1}{2}\sin[k_H(t_1^H+t_2^H)]\sin[k_L(t_1^L+t_2^L)](\frac{n_L^2k_H}{n_H^2k_L}+\frac{n_H^2k_L}{n_L^2k_H}) \\ & +\frac{1}{4}\cos[k_H(t_2^H-t_1^H)](\frac{n_L^2k_H}{n_H^2k_L}-\frac{n_H^2k_L}{n_L^2k_H})^2\sin(k_Lt_2^L)\sin(k_Lt_1^L)\end{aligned} \tag{17}$$

where $k_H = \sqrt{\left(\frac{n_H\omega}{c}\right)^2 - \beta^2}$ and $k_L = \sqrt{(n_L\omega/c)^2 - \beta^2}$. Here, ω, c and β represent the angular frequency of light, the light speed in the vacuum and the propagation constant in MB-1DPC, respectively. On the premise of making comprehensive consideration for the frequency ranges and the bandwidth of the two PBGs, the structural parameters can be set to $\Lambda_1 = 260$ nm, $\Lambda_2 = 380$ nm, $h_1 = t_1^H/\Lambda_1 = 0.5$, $N = 15$ and $h_2 = t_2^H/\Lambda_2 = 0.375$. Fig. 2 represents the omnidirectional total reflection in the dual-band range.

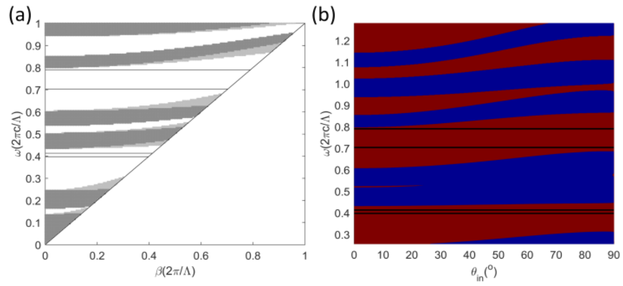

Fig. 2. (a) Photonic band-gap diagram of MB-1DPC. (b) The simplified reflectivity spectrum in terms of incident angle and the normalized frequency for TM polarization.

A band-gap diagram is usually used to investigate the PCs for an arbitrary angle as shown in Fig. 2(a). The deep and light gray regions indicate the allowed bands of TE and TM modes, respectively. Fig. 2(b) represents the simplified reflectivity spectrum in terms of incident angle and normalized frequency for TM polarization. The simplified reflectivity spectrum originates from the reflectivity spectrum, which is plotted as a function of incident angle and the normalized frequency for TM polarization by means of Eq. (15). The red area corresponds to $R \geq 99.999\%$ and the blue area corresponds to $R < 99.999\%$. The normalized frequencies of the dual-band range from 810nm to 910nm and from 1550nm to 1610nm for optical communication are marked by four black lines as shown in Fig. 2. It indicates that omnidirectional total reflection wavelength ranges in the simplified spectra agree well with that in photonic band diagram in MB-1DPC.

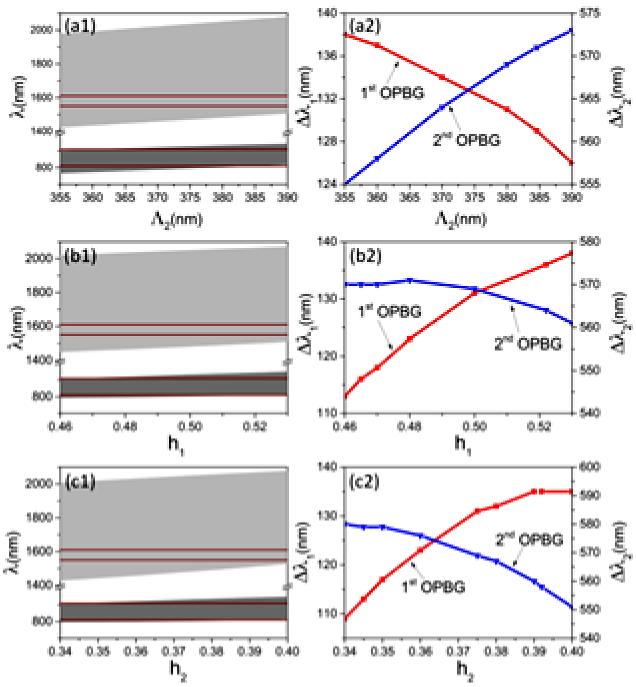

Fig. 3. The wavelength range and bandwidth of OPBGs versus: (a) Λ_2, (b) h_1 and (c) h_2.

Since the bandwidth of OPBGs for TM mode is narrower than the TE one apart from the normal incidence, the bandwidth of OPBGs in the PCs is determined by the TM mode. Fig. 3 illustrates the effect of h_1, h_2 and Λ_2 on the wavelength range and bandwidth of the two OPBGs for TM mode while the other parameters are consistent with the parameters in Fig. 2. The four purple horizontal lines as shown in Fig. 3(a1), (b1) and (c1) represent the dual-band range 810 nm ~ 910 nm and 1550 nm ~ 1610 nm for optical communication. The dark gray and light gray areas represent the first OPBG (1st OPBG) and the second OPBG (the 2nd OPBG), respectively. $\Delta\lambda_1$ and $\Delta\lambda_2$ represent the bandwidth of the 1st OPBG) and the 2nd OPBG, respectively.

Fig. 4 illustrates the effect of n_H, n_L and Λ_1 on the wavelength range and bandwidth of the two OPBGs for TM mode while the other parameters are consistent with the parameters in Fig. 2. In Fig. 4(a1), (b1) and (c1), the dual-band range 810 nm ~ 910 nm and 1550 nm ~ 1610 nm lies in 1st OPBG and 2nd OPBG, respectively.

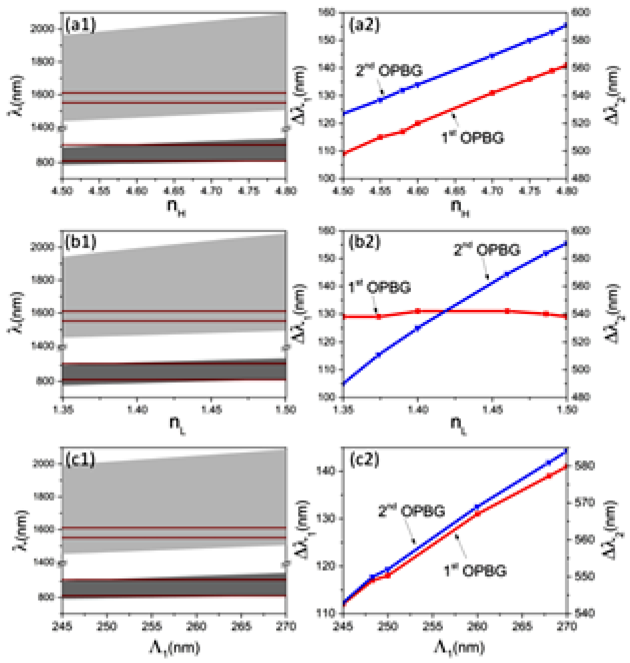

Fig. 4. The wavelength ranges and bandwidth of OPBGs versus: (a) n_H, (b) n_L and (c) Λ_1.

In Figs. 3 and 4, the increment of all the parameters can contribute to red shift of both upper band-gap edge (UBGE) and low band-gap edge (LBGE) in both the 1st OPBG and the 2nd OPBG, which is different from the heterostructured binary one-dimensional photonic crystal (HB-1DPC) [3]. In Ref. [3], the UBGE and LBGE are determined by structural parameters of S_1 and S_2, respectively. In order to achieve the omnidirectional reflection of the dual-band range, each parameter has its own feasible range while the remaining parameters are consistent with the parameters in Fig. 2. The feasible ranges of structural parameters in MB-1DPC are listed in Table 1.

Table 1. Feasible Ranges of Parameters in MB-1DPC

Λ_1 (nm)	248 ~ 268
Λ_2 (nm)	360 ~ 384
h_1	0.465 ~ 0.522
h_2	0.345 ~ 0.392
n_L	1.374 ~ 1.486
n_H	4.58 ~ 4.78

3.2. The Wavelength Range and Bandwidth of OPBGs in T-1DPC

In Eqs. (1) and (2), the $\mathrm{Re}(A_{TM})$ for TM mode and the $\mathrm{Re}(A_{TE})$ for TE mode in T-1DPC are given by

$$\begin{aligned}\mathrm{Re}(A_{TM}) = {} & \frac{1}{2k_H k_M k_L n_H{}^2 n_M{}^2 n_L{}^2}\cdot \\ & [2k_H k_M k_L n_H{}^2 n_M{}^2 n_L{}^2 \cos(k_H d_1^H)\cos(k_M d_1^M)\cos(k_L d_1^L) \\ & -k_H n_H{}^2(k_M{}^2 n_L{}^4 + k_L{}^2 n_M{}^4)\cos(k_H d_1^H)\sin(k_L d_1^L)\sin(k_M d_1^M) \\ & -k_L n_L{}^2(k_H{}^2 n_M{}^4 + k_M{}^2 n_H{}^4)\sin(k_H d_1^H)\cos(k_L d_1^L)\sin(k_M d_1^M) \\ & -k_M n_M{}^2(k_H{}^2 n_L{}^4 + k_L{}^2 n_H{}^4)\sin(k_H d_1^H)\cos(k_M d_1^M)\sin(k_L d_1^L)]\end{aligned} \tag{18}$$

$$\begin{aligned}\mathrm{Re}(A_{TE}) = {} & \frac{1}{2k_H k_M k_L}\cdot[2k_H k_L \cos(k_H d_1^H)\cos(k_L d_1^L) \\ & -(k_L k_H{}^2 + k_L k_M{}^2)\sin(k_H d_1^H)\sin(k_M d_1^M)\cos(k_L d_1^L) \\ & -(k_H k_M{}^2 + k_H k_L{}^2)\sin(k_H d_1^H)\sin(k_L d_1^L) \\ & -(k_M k_H{}^2 + k_M k_L{}^2)\sin(k_H d_1^H)\sin(k_L d_1^L)\cos(k_M d_1^M)]\end{aligned} \tag{19}$$

where $k_H = \sqrt{(n_H\omega/c)^2 - \beta^2}$, $k_M = \sqrt{\left(\frac{n_M\omega}{c}\right)^2 - \beta^2}$ a-nd $k_L = \sqrt{(n_L\omega/c)^2 - \beta^2}$. Here, β represents the propagation constant in T-1DPC.

On the premise of making comprehensive consideration for the frequency ranges and the bandwidth of the two PBGs, the structural parameters are $L_1 = 315$ nm, $a_1 = d_1^H/L_1 = 0.175$, $a_2 = d_1^M/L_1 = 0.285$ and $U = 20$. Fig. 5 represents the omnidirectional total reflection of the dual-band range.

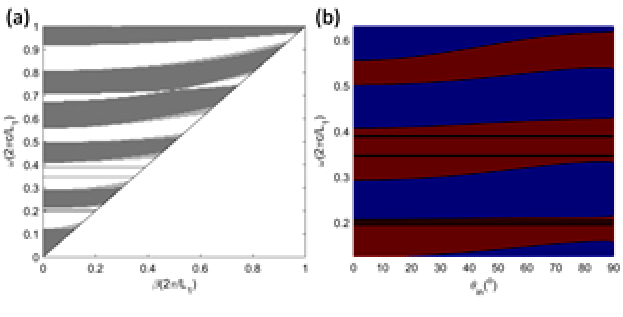

Fig. 5. (a) Photonic band-gap diagram of T-1DPC. (b) The simplified reflectivity spectrum in terms of incident angle and the normalized frequency for TM polarization.

In Fig. 5(a), the deep and light gray regions indicate the allowed bands of TE and TM modes, respectively. In Fig. 5(b), the red area corresponds to $R \geq 99.999\%$ and the blue area corresponds to $R < 99.999\%$.

In Fig. 5, the normalized frequencies of the dual-band range are marked by four dark lines. Fig. 5 indicates that omnidirectional total-reflection wavelength ranges in the simplified spectra agree well with that in photonic band diagram.

Fig. 6 illustrates the effect of n_H, n_M and n_L on the wavelength range and bandwidth of the two OPBGs while the other parameters are consistent with the parameters in Fig. 5. Fig. 7 illustrates the effect of L_1, a_1 and a_2 on the wavelength range and bandwidth of the two OPBGs while the other parameters are consistent with the parameters in Fig. 5.

In Figs. 6 and 7, the increment of all the parameters can contribute to redshift of both UBGE and LBGE in both the 1st OPBG and the 2nd OPBG. As shown in Fig. 6(c1), the increment of n_L can result in a significant red-shift on the UPGE wavelength of the 2nd OPBG, compared with the other three PGEs. In other words, the bandwidth of the 2nd OPBG can be greatly enhanced with n_L increasing when the other parameters are consistent with the parameters in Fig. 5. Fig. 7(a1) shows that the slight increase in L_1 can result in a smash red-shift on the PGEs wavelength in the two OPBGs, compared with the other five parameters. The feasible range of each parameter is listed in Table. 2

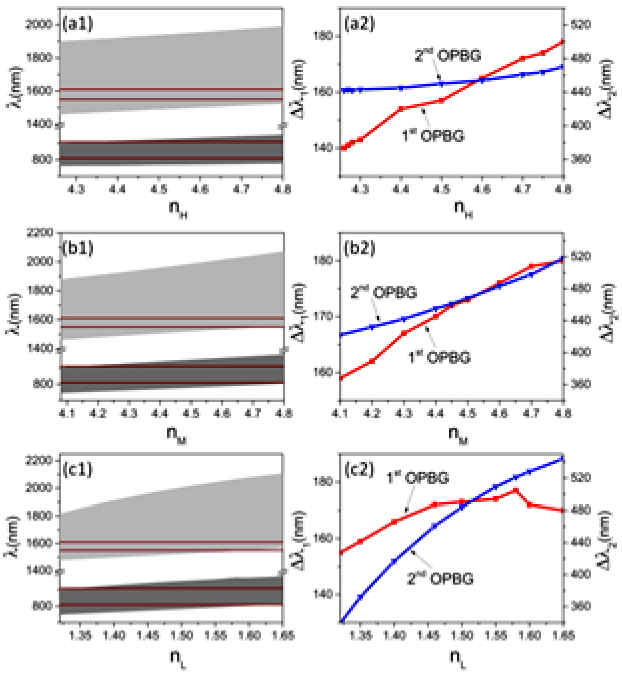

Fig. 6. The wavelength range and bandwidth of OPBGs versus: (a) n_L, (b) n_M and (c) n_H.

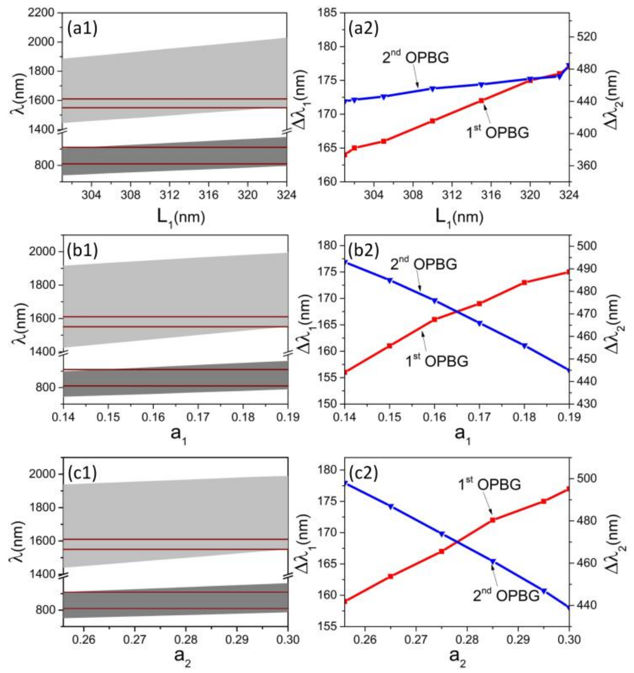

Fig. 7. The wavelength range and bandwidth of OPBGs versus: (a) L_1, (b) a_1 and (c) a_2.

Table 2. Feasible Ranges of Parameters in T-1DPC.

L_1 (nm)	303 ~ 323
n_L	1.34 ~ 1.60
n_M	4.14 ~ 4.74
n_H	4.33 ~ 4.80
a_1	0.147 ~ 0.190
a_2	0.256 ~ 0.300

3.3. Enlargement of the Two OPBGs Width by Using HT-1DPC

In order to broaden the bandwidth of the two OPBGs, the strategy of using HT-1DPC is adopted. The criterion for omnidirectional total reflection range enlargement by using heterostructure is the simultaneous adjacency of OPBGs [2, 3]. The reflectivity spectra and the simplified reflectivity spectra as a function of wavelength and incident angle for TM polarization is given in Fig. 8. The red area corresponds to $R \geq 99.999\%$ and the blue area corresponds to $R < 99.999\%$, as shown in Fig. 8(b).

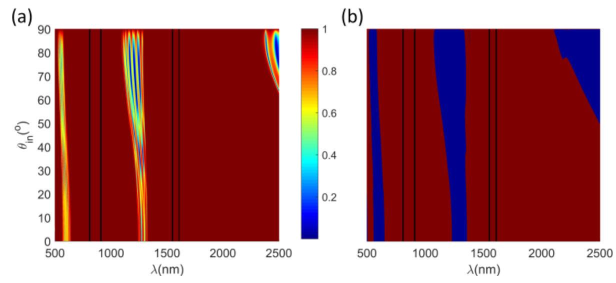

Fig. 8. (a) Reflectivity spectra and (b) simplified reflectivity spectra as a function of the wavelength and incident angle for the TM polarization with $L_1 = 360$ nm, $L_2 = 280$ nm, $a_1 = d_1^H/L_1 = d_2^H/L_2 = 0.175$, $a_2 = d_1^M/L_1 = d_2^M/L_2 = 0.285$, $U = 20$ and $N_g = 2$.

In Fig. 8, the dual-band range from 810 nm to 910 nm and from 1550 nm to 1610 nm, which are in the 1st OPBG and the 2nd OPBG, respectively. The bandwidths of the 1st OPBG and the 2nd OPBG are 420 nm and 722 nm, which are considerably enlarged for all angles for TM polarization, compared with the MB-1DPC (Figs. 3 and 4) and T-1DPC (Figs. 6 and 7). Fig. 8 indicates that the omnidirectional total reflection wavelength ranges can be greatly enhanced by means of HT-1DPC.

4. Analysis of reflectivity with material absorption

When the influence of the material absorption on the reflectivity of the reflector is considered, Eq. (6) can be modified to

$$\eta_i = \begin{cases} \sqrt{\widetilde{n_i^2} - n_A^2 \sin^2(\theta_{in})} \; for\ TE\ mode \\ \sqrt{\widetilde{n_i^2} - n_A^2 \sin^2(\theta_{in})/\widetilde{n_i^2}} \; for\ TM\ mode \end{cases} \quad (20)$$

where the complex refractive index $\widetilde{n_i}$ [37] has the form: $\widetilde{n_i} = n_i + ik_t$.

In order to achieve high reflectivity in the dual-band range 810 nm ~ 910 nm and 1550 nm ~ 1610 nm for optical communication, the material with the small value of k_t must be selected. On the premise of making comprehensive consideration for the materials with small absorption loss and the feasible ranges of structural parameters in Table 1 and Table 2, the B-1DPC and MB-1DPC are composed of Ge/PES, and the T-1DPC consists of Ge/Si/PES. The refractive indices of these materials [18, 36, 38] in B-1DPC, MB-1DPC, T-1DPC and HT-1DPC are summarized in Table 3. In the following discussions, the refractive indices of the air and the substrate are consistent with those described above.

Table 3. The Refractive Indices of the Materials.

Material	n_i	k_t
As_2Se_3	2.9	0.000001
PES	1.625	0.0001
Si	3.5	0.000001
Ge	4.5	0.06
SiO_2	1.45	0

4.1. Reflectivity of B-1DPC

The high and low refractive indices in B-1DPC are separately 4.5 and 1.625, which are different from the parameters (n_H, n_L) mentioned above. In this case, the simulation result is shown in Fig. 9. The minimum reflectivity in the dual-band range 810 nm ~ 910 nm and 1550 nm ~ 1610 nm for all incident angles is indicated by $R_{\min}$. Fig. 9 shows $R_{\min}$ is dependent on h and Λ with different k_t.

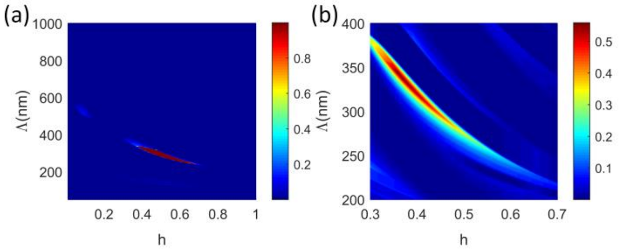

Fig. 9. R_{min} of B-1DPC structure for the TM polarization in terms of h and Λ with $n_L = 1.625$, $n_H = 4.5$, $n_A = 1.0$, $n_S = 2.9$ and $N = 20$. (a) $k_t = 0$ and (b) $k_t = 0.06$.

The purpose of Fig. 9(a) is to illustrate whether there are multiple regions [39] to achieve the omnidirectional reflection in the dual-band range. In this case, there is only one red area, which is different from Fig. 1 of Ref. [38] ,and values in the remaining areas cannot realize the omnidirectional total reflection in the dual-band range for B-1DPC. Fig. 9(b) represents $R_{\min}$ of B-1DPC for the TM polarization as a function of h and Λ with $k_t = 0.06$, which is the imaginary part of the refractive index of Ge. Since the imaginary part of the refractive indexes of PES and As_2Se_3 are tiny, the material absorption of the low refractive index layers and substrate can be ignored in B-1DPC. Owing to the large absorption of Ge, the maximum value of $R_{\min}$ in Fig. 9(b) can only reach 55.92% with the parameters summarized in Table 4. The number of periods contained in B-1DPC is donated by N.

Table 4. The Parameters of the Maximum R_{min} in B-1DPC.

Λ (nm)	344
k_t	0.06
n_L	1.625
n_H	4.5
N	20
h	0.36

Fig. 11 shows the effect of h_1 and h_2 on $R_{\min}$ for TM polarization By setting $\Lambda_1 = 260$ nm, $\Lambda_2 = 330$ nm, $N = 15$ and keeping the other parameters (n_L, n_H) the same as the parameters in Table 4.. Fig. 11(a) and (b) are separately plotted with $k_t = 0$ and $k_t = 0.06$, which are the imaginary part of the refractive index of Ge. In Fig. 10 and 11, the material absorption of the low refractive index layers and substrate can be ignored due to the tiny value of the imaginary part of the refractive indices of PES and As_2Se_3.

4.2. Reflectivity of MB-1DPC

By setting $h_1 = 0.545$, $N = 15$, $h_2 = 0.470$ and keeping the other parameters (n_L, n_H) the same as the parameters in Table 4. Fig. 10 shows the effect of Λ_1 and Λ_2 on $R_{\min}$ for TM polarization. Fig. 10(a) and (b) are separately plotted with $k_t = 0$ and $k_t = 0.06$, which are the imaginary part of the refractive index of Ge.

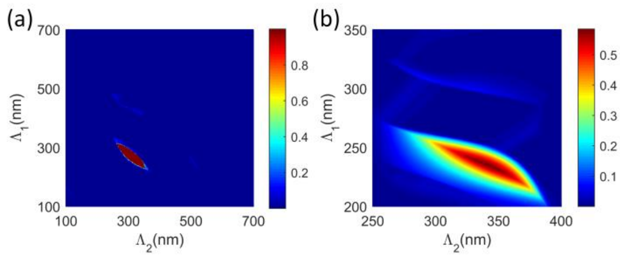

Fig. 10. R_{min} of MB-1DPC structure in terms of Λ_1 and Λ_2 for the TM polarization. (a) $k_t = 0$ and (b) $k_t = 0.06$.

Fig. 11 shows the effect of h_1 and h_2 on $R_{\min}$ for TM polarization By setting $\Lambda_1 = 260$ nm, $\Lambda_2 = 330$ nm, $N = 15$ and keeping the other parameters (n_L, n_H) the same as the parameters in Table 4. Fig. 11(a) and (b) are separately plotted with $k_t = 0$ and $k_t = 0.06$, which are the imaginary part of the refractive index of Ge. In Figs. 10 and 11, the material absorption of the low refractive index layers and substrate can be ignored due to the tiny value of the imaginary part of the refractive indices of PES and As_2Se_3.

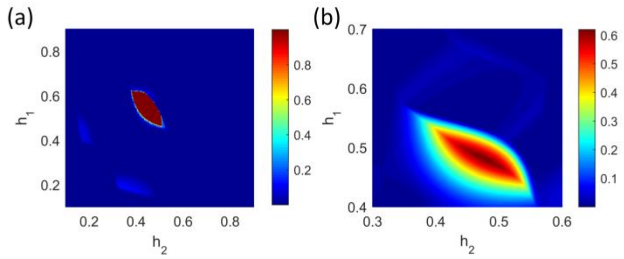

Fig. 11. R_{min} of MB-1DPC structure in terms of h_1 and h_2 for the TM polarization. (a) $k_t = 0$ and (b) $k_t = 0.06$.

In the case of non-absorption, the $R_{\min}$ in the red area tend to unity so that only the structural parameters in the red area can accomplish the omnidirectional total reflection of the dual-band range for TM mode, as shown in Fig. 10(a) and Fig. 11(a). In this case, there is only one red area where the omnidirectional total reflection can be achieved. In the case of the material absorption, the value of $R_{\min}$ can be greatly reduced, as shown in Fig. 10(b) and Fig. 11(b). Owing to the large absorption of Ge, the maximum value of $R_{\min}$ can only reach 61.89% in Fig. 11(b) for TM polarization with $\Lambda_1 = 260$ nm, $\Lambda_2 = 330$ nm, $h_1 = 0.482$, $h_2 = 0.476$, $N = 15$ and the other parameters (n_L, n_H, k_t) that are consistent with the parameters in Table 4.

4.3. Reflectivity of T-1DPC

Fig. 12(a) represents $R_{\min}$ is dependent on the a_1 and a_2 for TM mode by setting with $L_1 = 315$ nm, $n_M = 3.5$, $N_1 = 20$ and keeping the other parameters (n_L, n_H) the same as the parameters in Table 4. Fig. 12(a) and (b) are plotted with the imaginary part of the refractive index of Ge, i.e., $k_t = 0$ and $k_t = 0.06$, respectively.

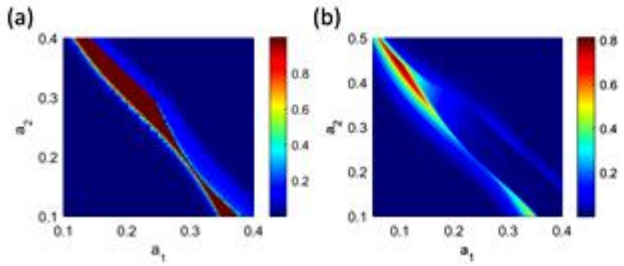

Fig. 12. R_{min} of T-1DPC structure in terms of a_1 and a_2 for the TM polarization. (a) $k_t = 0$ and (b) $k_t = 0.06$.

By setting $a_2 = 0.39$, $n_M = 3.5$, $U = 20$ and keeping parameters (n_L, n_H) the same as the parameters in Table 4, Fig. 13 shows the effect of L_1 and a_1 on $R_{\min}$ for TM polarization. Fig. 13(a) and (b) are separately plotted with $k_t = 0$ and $k_t = 0.06$, which are the imaginary part of the refractive index of Ge. Since the material absorption of PES and As_2Se_3 is scant compared with Ge, the optical loss in the PES and As_2Se_3 layers can be neglected in Fig. 12(b) and Fig. 13(b).

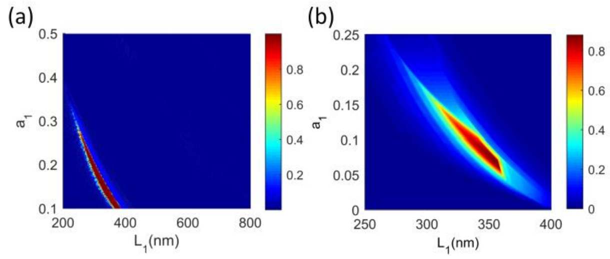

Fig. 13. R_{min} of T-1DPC structure in terms of L_1 and a_1 for the TM polarization. (a) $k_t = 0$ and (b) $k_t = 0.06$.

In the presence of the material absorption, the reflectivity of the T-1DPC in the dual-band range will drop, as shown in Fig. 12(b) and Fig. 13(d). The huge differences between Fig. 12(a) and (b) originate from the material absorption loss. From Fig. 13(b), the maximum value of $R_{\min}$ can reach 88.02% with $L_1 = 357$ nm, $n_M = 3.5$, $a_1 = 0.068$, $a_2 = 0.39$, $U = 20$ and the other parameters (n_L, n_H, k_t) that are consistent with the parameters in Table 4. By comparing T-1DPC with B-1DPC and MB-1DPC, it is found that the maximum value of $R_{\min}$ in T-1DPC is the highest when $k_t = 0.06$.

4.4. Reflectivity of HT-1DPC

Due to the large absorption of the materials, the three structures discussed above can't achieve high reflection in the dual-band range for optical communication. According to the discussion of HT-1DPC in Fig. 8, the bandwidth of the OPBGs can be significantly enhanced by adopting the strategy of simultaneous adjacency of OPBGs. Thus, the materials with bitty absorption loss can be selected to achieve the high reflection in the dual-band range. The HT-1DPC is composed of Si/As_2Se_3/PES, the refractive indices of which are listed in Table 4.

In the absence of the material absorption, Fig. 12(a) represents $R_{\min}$ of HT-1DPC for the TM polarization as a function of L_1 and L_2 by setting $n_H = 3.5$, $n_M = 2.9$, $a_1 = 0.165$, $a_2 = 0.365$, $N_g = 2$, $U = 20$ and keeping n_L the same as the parameters in Table 4. The reflectance is independent of the number N of the stratifications and the properties of the substrate, provided N is large enough [23]. In this case, the absorption loss of the substrate can be ignored. By keeping the parameters (a_1, a_2, n_M, n_L, n_H, U) the same as Fig. 14(a), Fig. 14(b) and (c) are plotted from the white dotted box in Fig. 14(a) with $k_t = 0.000001$ and $k_t = 0.0001$, respectively. By setting $L_2 = 425$ nm , $L_1 = 365$ nm and keeping the other parameters the same as Fig. 14(a), Fig. 14(d), (e) and (f) describe $R_{\min}$ is dependent on a_2 and a_1 with $k_t = 0$, $k_t = 0.000001$, $k_t = 0.0001$,respectively. In Fig. 14, all the imaginary parts of the refractive indices of the three materials are denoted by the same k_t.

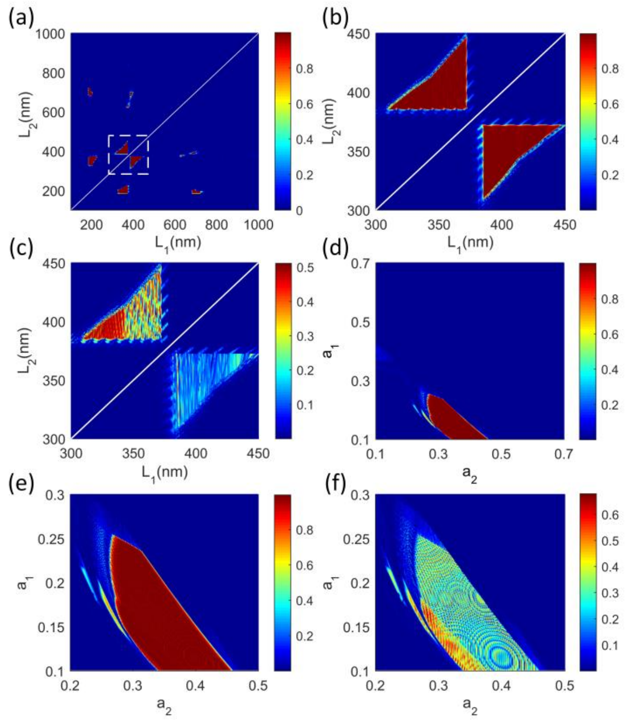

Fig. 14. R_{min} of HT-1DPC for the TM polarization as a function of L_1 and L_2: (a) $k_t = 0$, (b) $k_t = 0.000001$, (c) $k_t = 0.0001$. R_{min} of T-1DPC for the TM polarization in terms of a_2 and a_1: (d) $k_t = 0$, (e) $k_t = 0.000001$, (f) $k_t = 0.0001$.

Only the red areas in Fig. 14(a) can achieve the omnidirectional total reflection in the dual-band range for optical communication. In Fig. 14(a), the red areas are symmetrical about the white line, which is the angle bisector of the first quadrant. Compared with the B-1DPC, MB-1DPC and T-1DPC, the number of red areas in the HT-1DPC can reach up to ten in the case of non-absorption. Extra red areas provide more choices of parameter selection which can achieve the total reflection in the dual-band range so that an easy-processing structure can be selected in practical production.

According to Fig. 14(c), the distribution of $R_{\min}$ are not symmetrical about the white line. Compared with the value of $R_{\min}$ in Fig. 14(b) and (e), the value of $R_{\min}$ in Fig. 14(c) and (f) is drastically reduced, which means that $R_{\min}$ is remarkably affected by the value of k_t. In order to improve the reflectivity of the HT-1DPC in the dual-band range, the medium PES can be replaced with SiO_2, the material absorption of which can be ignored as shown in Table 3. With $a_1 = 0.262$, $a_2 = 0.208$, $n_L = 1.45$ and the other parameters (n_M, n_L, n_H, U) that are consistent with Fig. 14(e), the maximum of $R_{\min}$ in the HT-1DPC composed of $Si/As_2Se_3/SiO_2$ can reach up to 99.62% by means of Eqs. (15) and (20). The maximum values of $R_{\min}$ in B-1DPC, MB-1DPC, T-1DPC and HT-1DPC are summarized in Table 5. In particular, the reflectivity in HT-1DPC are the highest among these structures and reach 99.62%, which is comparable to the reflectivity in recent works [40-41].

Table 5. the Maximum Values of R_{min} in the Four Structures

B-1DPC (Ge/PES)	55.92%
MB-1DPC (Ge/PES)	61.89%
T-1DPC (Ge/Si/PES)	88.02%
HT-1DPC ($Si/As_2Se_3/SiO_2$)	99.62%

5. Comparison of reflectivity between TE mode and TM mode

In the presence of the material absorption, the omnidirectional total in the dual-band range cannot be achieved. In order to achieve the omnidirectional high reflection of the PCs, one must have omnidirectional high reflection for both polarization states. Figs. 15 and 16 are plotted for TE mode and TM mode with the parameters that can achieve the maximum values of $R_{\min}$ in B-1DPC, MB-1DPC, T-1DPC and HT-1DPC, which are listed in Table 5.

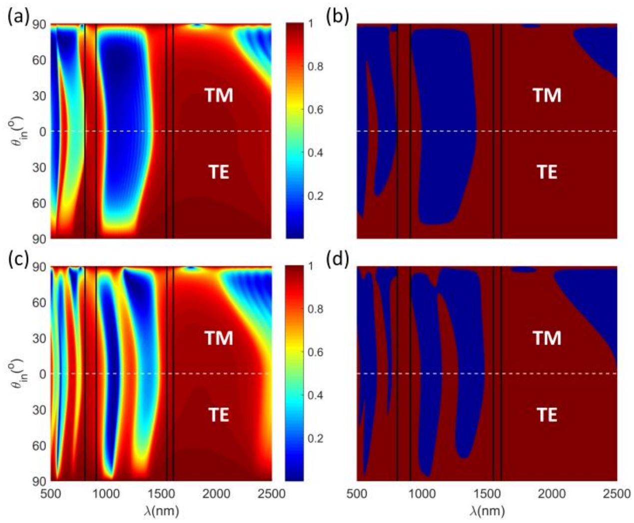

Fig. 15. (a) Reflection spectrum and (b) simplified refection spectrum as a function of incident angle and wavelength for TM and TE polarization state with the parameters of B-1DPC summarized in Table 4. (c) Reflection spectrum and (b) simplified refection spectrum as a function of incident angle and wavelength for TM and TE polarization state with the parameters that can achieve the maximum value of R_{min} in MB-1DPC.

Fig. 15(a) and (c) show the reflection spectra as a function of incident angle and wavelength for TE mode and TM mode in B-1DPC and MB-1DPC, respectively. The four black lines represent the dual-band range from 810 nm to 910 nm and from 1550 nm to 1610 nm for optical communication. In Fig. 15(b), the red area corresponds to $R \geq 55.92\%$ and the blue region corresponds to $R < 55.92\%$. Fig. 15(b) shows the reflectivity in the dual-band range for TE mode is not less than the maximum values of $R_{\min}$ in B-1DPC. The red zone in Fig. 15(d) corresponds to $R \geq 61.89\%$ and the blue region corresponds to $R < 61.89\%$. The dual-band range for optical communication is still located in the red zone for TE mode as shown in Fig. 15(d). In other words, the maximum of $R_{\min}$ for TE polarization is not less than the one for TE polarization in B-1DPC and MB-1DPC.

Fig. 16(a) and (c) describe the reflection spectra as a function of incident angle and wavelength for TM polarization and TE polarization in the T-1DPC and HT-1DPC, respectively. The red area in Fig. 16(b) and (d) correspond to $R \geq 88.02\%$ and $R \geq 99.62\%$, respectively.

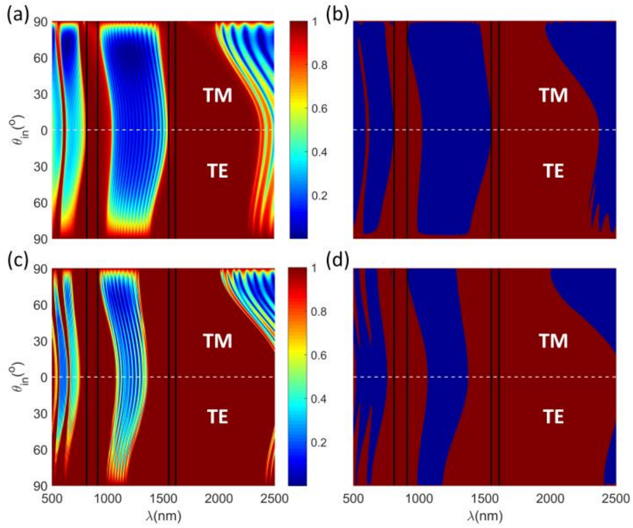

Fig. 16. (a) Reflection spectrum and (b) simplified reflection spectrum as a function of incident angle and wavelength for TM and TE polarization state with the parameters that can achieve the maximum value of R_{min} in T-1DPC. (c) Reflection spectrum and (d) simplified reflection spectrum as a function of incident angle and wavelength for TM and TE polarization state with the parameters that can achieve the maximum value of R_{min} in HT-1DPC.

The dual-band range for optical communication lies in the red region for the TE mode as shown in Fig. 16(b) and (d). Namely, the maximum of $R_{\min}$ is not less than 88.02% for the TE mode in the T-1DPC and not less than 99.62% for the TE mode in the HT-1DPC. Since the maximum of $R_{\min}$ for TE polarization is not less than the TM one, the highest reflectivity for both polarization states that can be achieved in the dual-band range from 810 nm to 910 nm and from 1550 nm to 1610 nm in the B-1DPC, MB-1DPC, T-1DPC and HT-1DPC structure is determined by the TM polarization.

6. Conclusions

In summary, the MB-1DPC, T-1DPC and HT-1DPC are investigated to achieve the omnidirectional total reflection in the dual-band range from 810 nm to 910 nm and from 1550 nm to 1610 nm for optical communication without the material absorption being considered. The frequency ranges of the OPBGs in simplified reflection spectra agree well with the PBGs frequency ranges in photonic band diagram. The effects of the structural parameters on the shifts and bandwidth of the two OPBGs in MB-1DPC and T-1DPC have been discussed. The bandwidth of the two OPBGs can be significantly enhanced by using HT-1DPC. Since the bandwidth of the two OPBGs can be significantly enhanced by means of HT-1DPC, more materials can be employed which means the materials with bitty absorption loss can be selected to achieve high reflection in the dual-band range. The highest reflectivity in HT-1DPC composed of Si/As_2Se_3/SiO_2 can reach up to 99.62%. Since the maximum reflectivity that can be achieved in each structure for TE mode is not less than the TM mode in the dual-band range, the maximum value of reflectivity in each structure that can be achieved in the dual-band is determined by the TM polarization.

Acknowledgment

This work is supported by the National Natural Science Foundation of China (Grant No. 11574042).

References

[1] P. Yeh, A. Yariv, E. Maron, J. Opt. Soc. Am. **68**, 1196(1978).
[2] Xin Wang, Xinhua Hu, Yizhou Li, Wulin Jia, Chun Xu, Xiaohan Liu, Jian Zi, Appl. Phys. Lett. **80**, 4291 (2002).
[3] Peng Han, Hezhou Wang, J. Opt. Soc. Am. B **22**, 1571 (2005).
[4] Li-Gang Wang, Hong Chen, and Shi-Yao Zhu, Phys. Rev. B **70**, 245102 (2004).
[5] Haitao Jiang, Hong Chen, Hongqiang Li, Yewen Zhang, Appl. Phys. Lett. **83**, 5386 (2004).
[6] Limei Qi, Ziqiang Yang, Feng Lan, Xi Gao, Zongjun Shi, Physics of Plasmas **17**, 042501 (2010).
[7] Hai-Feng Zhang, Shao-Bin Liu, Xiang-Kun Kong, Liang Zou, Chun-Zao Li, Wu-shu Qing, Physics of Plasmas **19**, 022103 (2012).
[8] I. El-Kady, M. M. Sigalas, R. Biswas, K. M. Ho, C. M. Soukoulis, Phys. Rev. B **62**, 15299 (2000).
[9] Zhi-Yuan Li, Ben-Yuan Gu, Guo-Zhen Yang, Phys. Rev. Lett. **81**, 2574 (1998).
[10] Young-Chung Hsue, Arthur J. Freeman, Ben-Yuan Gu, Phys. Rev. B **72**, 195118 (2005).
[11] G. Alagappan, X. W. Sun, P. Shum, M. B. Yu, M. T. Doan, J. Opt. Soc. Am. B **23**, 159 (2006).
[12] Bipin K. Singh, Mayank K. Chaudhari, Praveen C. Pandey, J. Lightwave Technol. **34**, 2431 (2016).
[13] Hamza Kurt, David S. Citrin, Opt. Express **15**, 1240 (2007).
[14] M. Turduev, B. B. Oner, I. H. Giden, H. Kurt, J. Opt. Soc. Am. B **30**, 1569 (2013).
[15] Sang, Zhi-Fang, Zhen-Ya Li, Optics Communications. **259**, 174 (2006).

[16] H. Kurt, E. Colak, O. Cakmak, H. Caglayan, E. Ozbay, Appl. Phys. Lett. **93**, 171108 (2008).
[17] J. A. E. Wasey, W. L. Barnes, J. Mod. Opt. **47**, 725 (2000).
[18] Dora Juan Juan Hu, Gandhi Alagappan, Yong-Kee Yeo, Perry Ping Shum, Ping Wu, Opt. Express **18**, 18671 (2010).
[19] Y. Y. Wang, N. V. Wheeler, F. Couny, P. J. Roberts, F. Benabid, Opt. Lett. **36**, 669 (2011).
[20] G. Bouwmans, L. Bigot, Y. Quiquempois, F. Lopez, L. Provino, M. Douay, Opt. Express **13**, 8452 (2005).
[21] S. Février, R. Jamier, J.-M. Blondy, S. L. Semjonov, M. E. Likhachev, M. M. Bubnov, E. M. Dianov, V. F. Khopin, M. Y. Salganskii, A. N. Guryanov, Opt. Express **14**, 562 (2006).
[22] I. Abdulhalim, Opt. Commun. **215**, 225 (2003).
[23] J. Lekner, J. Opt. **16**, 035104 (2014).
[24] Jianyu Guo, Ping Jiang, Huajun Yang, Ye Niu, Jiawei Xianyu, Appl. Opt. **56**, 2455 (2017).
[25] Li Zhang, Lu Chen, HuaJun Yang, Ping Jiang, Shengqian Mao, Weinan Caiyang, Appl. Opt. **54**, 7148 (2015).
[26] Weinan Caiyang, Huajun Yang, Ping Jiang, Wensen He, Yu Tian, Xue Chen, Appl. Opt. **56**, 5080 (2017).
[27] J. O. Estevez, J. Arriaga, A. Méndez Blas, et al, Appl. Phys. Lett. **94**, 061914 (2009).
[28] Suneet Kumar Awasthi, Usha Malaviya, Sant Prasad Ojha, J. Opt. Soc. Am. B **23**, 2566 (2006).
[29] Ebrahimi, Vahid, Leila Yousefi, Mahmoud Mohammad-Taheri. Opt. Commun. **82**, 119 (2017).
[30] Lichao Shi, Wei Zhang, Jie Jin, Yidong Huang, Jiangde Peng, J. Lightwave Technol. **30**, 1492 (2012).
[31] Yong Xu, Reginald K. Lee, Amnon Yariv, Opt. Lett. **25**, 1756 (2000).
[32] J. N. Winn, Y. Fink, S. Fan, J. D. Joannopoulos, Opt. Lett. **23**, 1573 (1998).
[33] Y. Fink, J. N. Winn, S. Fan, C. Chen, J. Michel, J. D. Joannopoulos, E. L. Thomas, Science **282**, 1679 (1998).
[34] Moriaki Wakaki, Keiei Kudo, Takehisa Shibuya, Physical Propertiesand Data of Optical Material, CRC Press, New York p. 251, 2007.
[35] Moriaki Wakaki, Keiei Kudo, Takehisa Shibuya, Physical Propertiesand Data of Optical Material, CRC Press, New York p. 243, 2007.
[36] Guangyu Xu, Wei Zhang, Yidong Huang, Jiangde Peng, J. Lightwave Technol. **25**, 359 (2007).
[37] Liang Shang, Xiuqin Yang, Yunjie Xia, Hengliang Wang, J. Lightwave Technol. **32**, 1717 (2014).
[38] Moriaki Wakaki, Keiei Kudo, Takehisa Shibuya, Physical Properties and Data of Optical Material, CRC Press, New York p. 165, 2007.
[39] A. G. Barriuso, J. J. Monzón, L. L. Sánchez-Soto, A. Felipe, Opt. Express **13**, 3913 (2005).
[40] S. Sahel, et al, Superlattices and Microstructures **111**, 1 (2017).
[41] Wang Xian, et al, Journal of Alloys and Compounds **697**, 1 (2017).

*Corresponding author: yanghj@uestc.edu.cn